Available online at www.sciencedirect.com
ScienceDirect
International Journal of Heat and Mass Transfer 51 (2008) 1757–1769
International Journal of HEAT and MASS TRANSFER
www.elsevier.com/locate/ijhmt

Thermal analysis of a wet-disk clutch subjected to a constant energy engagement

Tien-Chen Jen *, Daniel James Nemecek

Mechanical Engineering Department, University of Wisconsin-Milwaukee, Milwaukee, WI 53211, United States

Received 23 March 2007; received in revised form 6 July 2007
Available online 12 September 2007

Abstract

A combined theoretical and experimental thermal analysis is conducted on the plates within a wet clutch for one engagement. An analytical model using the separation of variables technique is developed to simulate the temperature rise due to the non-conservative friction and relative motion between the steel plates and friction plates of the clutch. A complimentary numerical model is also developed to compute the temperature distribution in the steel plate. The experiment performed included a wet clutch instrumented with thermocouples and installed in a power-shift transmission where the temperature rise during one clutch engagement was measured. The total energy is then estimated by accounting for system inertia, torque and rotating speeds. Finally, the temperature rises predicted by the analytical and numerical models are validated with the experimental data.

1. Introduction

High power rated automatic transmissions are widely used in engineering applications involving large agricultural tractors and off-highway vehicles, such as military transport and crash-fire rescue trucks. An automatic transmission, also known as a power-shift transmission, includes numerous elements involved in the transmission of energy and provides the necessary torque to perform the mechanical work given a particular operating condition. The changing of transmission output torque is accomplished by taking the input shaft speed of the transmission and providing a modified output speed via the fixed ratio gear trains. The element obligated to synchronize these speeds while changing gear ratios is the wet clutch assembly.

The wet clutch assembly consists of multiple friction plates and steel plates, with clamp force imparted by a hydraulic piston. When the clutch is disengaged, the friction and steel plates rotate independent of each other. The core of the friction plate and the steel plate is typically made from plain carbon steel. Each friction plate face is lined with a paper-based, bronze-based or carbon fiber materials. The steel plates are mated to one splined member (i.e. shaft, hub, gear ring, etc.) and the friction plates are mated to a second splined member. The engagement process begins when hydraulic pressure is applied to one side of the piston resulting in axial movement along the shaft. Sufficient hydraulic pressure is applied to compress the friction and steel plates, therefore eliminating the relative rotational speeds and causing the corresponding gears and shafts to rotate at constant fixed ratios.

The process of engagement is divided into three stages. The first stage, often called the "hydrodynamic stage" or "squeeze stage", involves no contact between the friction and steel plates while each plate is separated by a film of fluid. Torque that might be transferred through the clutch during this stage is done through the viscous shear of the oil, and fluid motion is governed by the theory of hydrodynamic lubrication. But typically the inertia load is significant enough to resist friction plate rotation and thus torque transfer. The second stage, called "boundary lubrication stage" or "squash stage", begins when hydraulic

* Corresponding author. Tel.: +1 414 229 2307; fax: +1 414 229 6958.
E-mail address: jent@uwm.edu (T.-C. Jen).

0017-9310/$ - see front matter © 2007 Elsevier Ltd. All rights reserved.
doi:10.1016/j.ijheatmasstransfer.2007.07.009

Nomenclature

a	constant, Eq. (18)
A	coefficient in numerical analysis, Eq. (27)
A_m	constant in series solution, Eq. (10)
A_{mn}	constant in series solution, Eq. (17)
B_m	constant in series solution, Eq. (10)
b	constant, Eq. (18)
c_p	specific heat (J/kg/K)
C	cylinder function defined in Eq. (11)
e	energy dissipation rate (W/s), Eq. (33)
E	total energy dissipation (W), Eq. (34)
f	fraction of heat entering steel plate (W), Eqs. (24) and (25)
F	clutch engagement force (N), Eq. (34)
H	plate thickness (mm)
I	inertia (kg m^2)
J_n	Bessel function of first kind
k	thermal conductivity (W/m/K)
N	number of friction surfaces
q	heat flux (W/m^2)
r	radius or radial direction (mm)
R	function of r defined in Eq. (6)
S	heat partition factor, Eq. (25)
T	torque (N m)
t	time (s)
U	uncertainty
Y_n	Bessel function of second kind
z	axial direction (mm)
Z	function of$z$ defined in Eq. (6)

Greek symbols

α	thermal diffusivity (m^2/s)
γ	eigenvalue
e	error percentage of convergence test
h	eigenvalue
ρ	density (kg/m^3)
μ	dynamic coefficient of friction
Θ	temperature (°C)
F	function of time defined in Eq. (5)
w	rotational speed (rad/s)

Subscripts

ave	average
d	dynamic torque clutch capacity
E	east of point in axial direction
f	friction plate
i	inside
in	input
N	north of point in radial direction
o	outside
out	output
m	variable index
n	variable index
P	point of analysis
s	steel plate
S	south of point in radial direction
W	west of point in axial direction
0	Bessel function order
1	Bessel function order

Superscripts

k	time step index
“	heat flux index

pressure is applied to the piston and the asperities of the friction material contact the steel plate. The majority of the torque transferred through the clutch during this stage is done at the points of material contact and not through the oil shear. The third stage, known as the “full mechanical contact” or “lock-up” stage, is reached when no relative motion exists between the plates. This stage has no heat generation between the plates, and the plates begin to cool as heat is transferred to the oil passing through the grooves of the friction material.

During the boundary lubrication stage of engagement, the kinetic energy of the relative motion is absorbed during the slippage in the form of heat until no relative motion exists. Although undesirable from a thermal standpoint, this slippage is necessary to allow for the gradual acceptance of the load by the prime mover without stalling or shocking the system with a rapid acceleration. Shigley and Mischke [1] state that torque capacity is limited by the characteristics of the material and the ability of the clutch to dissipate heat. If the heat is generated during the synchronizing period faster than it is dissipated, the temperature rise in the plates will cause thermal failure of the clutch. Several different modes of thermal failure are identified by Anderson and Knapp [2] as coning, “hot spotting” of the steel plates, smearing of the friction material on the mating steel plate and excessive oil temperature leading to the breakdown of its properties.

Parameters of wet clutch design focus on torque capacity and engagement time. Payvar [3] states that nearly all the heat generated during a “typical” engagement, where slip time lasts from 0.2 to 2.0 s, is absorbed by the steel plates. A negligible amount of heat is transferred to the oil flowing between asperity contact points and though the grooves in the friction material. For cases where the clutch modulates the transmission output speed to slowly accelerate significant loads relative to its design capacity, slip times often exceed 5.0 s or greater. In these cases plate temperatures will reach a steady state value after a few seconds given an adequate oil flow to dissipate the heat. The steady state temperature of the plates in this case is depen-

dent on the heat transfer coefficient of the oil. In addition, friction plate temperatures cannot be neglected in extended engagement cases and when higher conductivity materials are used on the friction plate surface.

In early thermal analysis studies of wet clutch systems (e.g., [4,5]), empirical models were developed from experimental methods and simplified one-dimensional analytical models of heat conduction between plates. A more comprehensive analysis was done by Schade [6] with an improved finite difference numerical scheme and confirmed experimentally by measuring the temperature rise due to friction in the transmission. El-Sherbiny and Newcomb [7] simulated the clutch engagement with a finite element model that included the hydrodynamic effect. Zagrodzki [8,9] numerically calculated the temperature fields and the thermal stress distribution of steel plates within a multi-disc clutch and analyzed the thermal effects of the normal hydraulic pressure distribution on the plates. The most comprehensive numerical studies to date were performed by Natsumeda and Miyoshi [10], complemented with additional considerations by Jang and Khonsari [11]. Notable factors included were surface-roughness, friction lining permeability and waviness, fluid viscous dissipation effects and friction material groove effects. However, simulations of clutch engagements to produce temperature gradients within the steel plates were not validated with an experiment. Energy and fluid flow governing equations within a wet clutch were coupled and solved simultaneously with finite difference techniques by Yang et al. [12]. The temperature gradients and resulting heat transfer were determined, and compared favorably with the measured interface temperatures.

More recent analysis of a wet clutch was completed by Tatara and Payvar [15] expanded on work previously done by Payvar and Majumdar [16], and numerically determined the convective heat transfer coefficient for the oil in various friction plate groove patterns. A finite volume approach was used in this case [15] and a validated with experimental data. A finite volume approach was also used by Lai [17] in developing a full three-dimensional thermal model for predicting the transient response of a clutch pack. These cases [15–17] were all highly complex models validated with a simplified typical experimental setup.

The objective of this paper is to analyze the transient temperature response within a wet-clutch system for one "typical" engagement of a power-shift transmission. Based on the sensitivity of the steel plate to thermal failure (i.e. buckling, coning or focal hot spotting) due to its higher thermal load relative to the friction plate, an analysis of the temperature field of a steel plate will be done analytically, numerically and experimentally. From all earlier studies regarding wet-clutch thermal energy analysis, none have been found with experimental data collected from wet clutches coupling a continuously rotating driver to a driven inertia free to rotate (i.e., the objective of an automotive transmission clutch). Often tests simulate the clutch action by locking the output and operating the clutch as a brake. For instance, experimental works done by Johnson [13] and Pacey [14] on a power-shift transmission clutch used this method. Although the brake action does simulate the lock-up action of a clutch, dynamic characteristics of the system during a typical clutch engagement can not be seen which may affect thermal energy studies.

Details of this study include an engagement process where it is assumed that the temperature fields are axis-symmetric, leading to a two-dimensional model (radial and axial). The two-dimensional transient governing equation for the heat conduction will be solved both analytically and numerically given experimental heat energy input data. The surface temperature of the steel plate at the mean radius is collected during the experiment. Then, a simple model is developed to estimate the energy partition into each plate. Once the energy partition is known, the heat flux input into the steel plates can be calculated and then be used in the analytical and numerical calculations to determine the temperature fields in the steel plate. All three results are then compared.

2. Analytical model

In a wet-clutch system, the heat generation is due to the relative motion between the friction and steel plates of a power-shift transmission during engagement. Fig. 1 shows the cross-sectional view of the transmission with the clutches noted. The engagement process occurs within each clutch under required operating conditions.

Considering the geometry of the plates (see Fig. 2), the governing heat conduction equation in cylindrical coordinates is as follows:

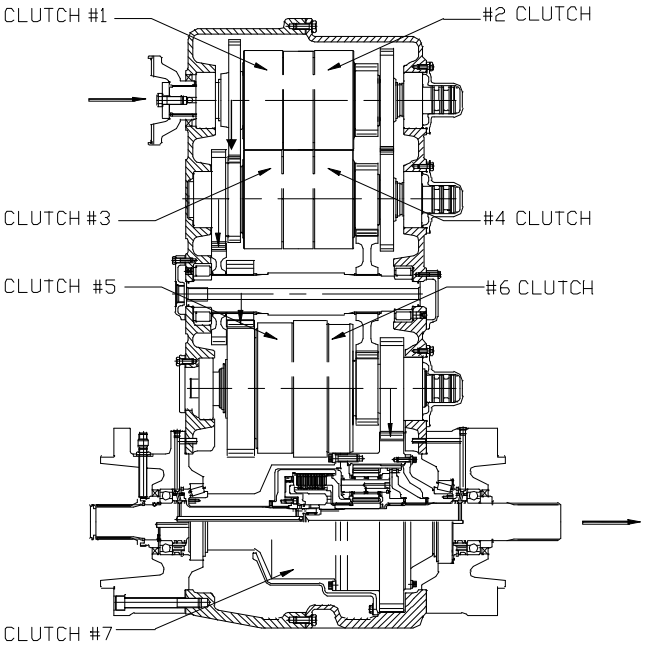

Fig. 1. Subject power-shift transmission.

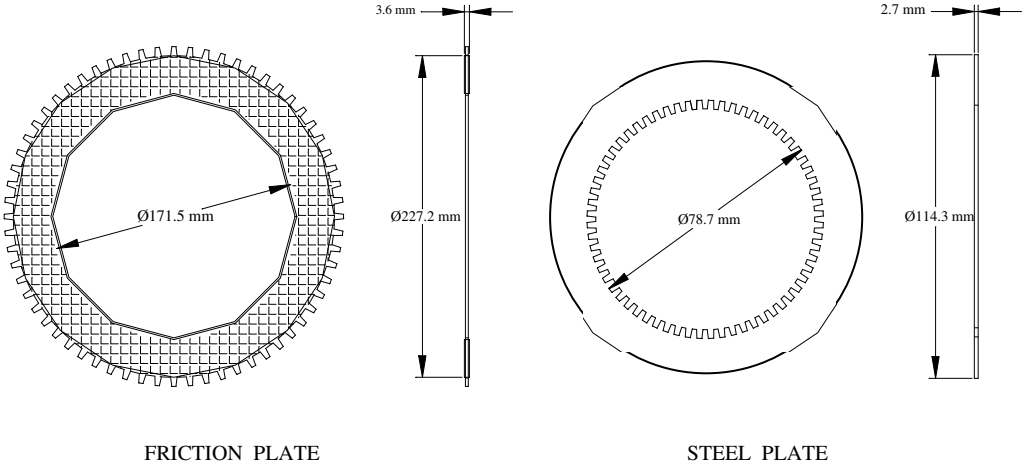

Fig. 2. Subject transmission plates.

$$\rho c_{\mathrm{p}} \frac{\partial \Theta}{\partial t} = k\left(\frac{\partial^2 \Theta}{\partial r^2} + \frac{1}{r}\frac{\partial \Theta}{\partial r} + \frac{\partial^2 \Theta}{\partial z^2}\right) \tag{1}$$

The thermal property for each material considered here is assumed constant and the temperature variation in the angular direction is assumed to be negligible. This was justified by Schade [6] and further supported by the fact of the relatively low temperature rises in the experimental engagements performed. It is further assumed that both steel plate and friction plate can be approximated by concentric cylinders (i.e., without gear teeth).

Only the plate engagement is considered in this study. The boundary conditions for this case can be assumed to be adiabatic at the inside and outside radius surfaces of the steel plate (see Eq. (2)). The two steel plate surfaces that are in contact with the friction plates are assumed to have a given constant heat flux boundary condition (see Eq. (2)).

$$\frac{\partial \Theta}{\partial r}(R_i, z, t) = 0, \quad \frac{\partial \Theta}{\partial r}(R_{\mathrm{o}}, z, t) = 0, \quad k\frac{\partial \Theta}{\partial z}(r, 0, t) = -q_1'',$$
$$k\frac{\partial \Theta}{\partial z}(r, H, t) = q_2'', \quad \Theta(r, z, 0) = \Theta_{\mathrm{o}} \tag{2}$$

It can be seen that the boundary conditions are non-homogenous due to the heat inputs into the steel plates from the axial contact surfaces. In order to apply the method of separation of variables in solving the governing equation, the following general form of solution is applied:

$$\Theta = \Theta^* - az - bz^2 - ct \tag{3}$$

Within Eq. (3), the temperature term Θ^*, constitutes the homogenous solution, while the additional terms account for the non-homogeneous boundary conditions and prevent a runaway solution. Applying Eq. (3) to the non-homogenous boundary conditions, Eq. (2), and letting the boundary conditions become homogeneous, the solutions for the values of a, b and c are found to be:

$$a = \frac{q_1''}{k}, \quad b = -\frac{(q_1'' + q_2'')}{2kH}, \quad c = \frac{2kb}{\rho c_{\mathrm{p}}} \tag{4}$$

Now that the non-homogenous boundary conditions have been dealt with, the non-homogenous boundary conditions can be set equal to zero with Θ replaced by Θ^* and the initial condition becomes:

$$\Theta^*(r, z, 0) = \Theta_0 + az + bz^2 \tag{5}$$

The assumed homogenous solution Eq. (5) can then be applied to Eq. (1) as follows:

$$\Theta^* = \Theta^*(r, z, t) = R(r)Z(z)\Phi(t) \tag{6}$$

The assumed solution is then differentiated with respect to r, z and t as needed to substitute into Eq. (1). Upon separation of variables it is seen that a function of t is equal to a function of r plus a function of z. The only way functions of r and functions of z can be equated to a function of t is if they are constant. The function of r and function of z can be rewritten as two ordinary differential equations:

$$\left[\frac{R''(r)}{R(r)} + \frac{1}{r}\frac{R'(r)}{R(r)}\right] = -\eta^2, \quad \frac{Z''(z)}{Z(z)} = -\gamma^2 \tag{7}$$

The first differential equation in Eq. (7) can be solved in the form of the Bessel Equation, with the known general solution to be:

$$R(r) = AJ_0(\eta r) + BY_0(\eta r) \tag{8}$$

When the boundary conditions are applied to Eq. (8), two homogeneous algebraic equations are formed. In order for the solutions to exist, Cramer's rule was used, which states that the denominator component of the determinant of the two equations must equal zero, leading to the eigen-condition as follows:

$$J_1(\eta R_{\mathrm{i}})Y_1(\eta R_{\mathrm{o}}) - J_1(\eta R_{\mathrm{o}})Y_1(\eta R_{\mathrm{i}}) = 0 \tag{9}$$

Note that Eq. (9) is solved numerically to find the eigenvalues η_m. Now the solution in the r direction, $R_m(r)$, can be written as

$$R_m(r) = A_m J_0(\eta_m r) + B_m Y_0(\eta_m r) \tag{10}$$

The Bessel functions of the first and second kind combined as in Eq. (10) can be rewritten using the definition of a cylinder function:

$$C_0(\eta_m r) = J_0(\eta_m r) + DY_0(\eta_m r) \tag{11}$$

$$\text{where : } D = \frac{B_m}{A_m} = -\frac{J_1(\eta_m R_o)}{Y_1(\eta_m R_o)} = -\frac{J_1(\eta_m R_i)}{Y_1(\eta_m R_i)}$$

Therefore, the expression for R_m can be written as

$$R_m = C_0(\eta_m^r) \quad \text{for } m = 1, 2, 3, \ldots \tag{12}$$

Note that any constant within the expression for R_m is absorbed in the constant for the entire homogenous solution, Eq. (6).

The ordinary differential equation for $Z(z)$ in Eq. (7) can be written in the form:

$$Z''(z) + \gamma^2 Z(z) = 0 \tag{13}$$

After applying the homogeneous boundary conditions to Eq. (13), the eigenfunction and corresponding eigenvalues can be written as follows:

$$Z_n(z) = \cos(\gamma_n z), \quad \gamma_n = \frac{(n-1)\pi}{H}, \quad \text{for } n = 1, 2, 3, \ldots \tag{14}$$

The expressions for $R_m(r)$ and $Z_n(z)$ can now be used to find an expression for $\Theta(t)$. By substituting Eq. (3) into the governing equation (Eq. (1)), the governing equation takes the following form:

$$\begin{aligned}\frac{1}{\alpha}\sum_m^\infty\sum_n^\infty R_m(r)Z_n(z)\Phi_{mn}^{(}t) &= \sum_m^\infty\sum_n^\infty R_m''(r)Z_n(z)\Phi_{mn}(t) + \frac{1}{r}R_m'(r)Z_n(z)\Phi_{mn}(t) \\ &\quad + R_m(r)Z_n''(z)\Phi_{mn}(t)\end{aligned} \tag{15}$$

Since the R_m and Z_n are eigenfunctions and are orthogonal functions, an ordinary differential equation for $\Phi(t)$ can be found by applying orthogonality to Eq. (15). This leads to the following equation:

$$\frac{d\Phi_{mn}}{dt} = -\alpha(1+\gamma_n^2)\Phi_{mn} \tag{16}$$

The general solution to this differential equation is:

$$\Phi_{mn}(t) = A_{mn}e^{-\alpha(1+\gamma_n^2)t} \tag{17}$$

In order to determine the coefficient A_{mn}, the assumed solution of Eq. (3) is rearranged and equated to the terms of the homogeneous solution Q^*.

$$\Theta^* = \sum_m^\infty\sum_n^\infty R_m(r)Z_n(z)\Phi_{mn}(t) = \Theta + az + bz^2 + ct \tag{18}$$

When the initial condition is applied, the last term on the right side is dropped and $\Phi_{mn}(0)$ is treated as a constant.

for $n = 1$:

$$A_{mn} = \frac{\left(\Theta_o H + \frac{3}{2}aH^2\right)\left(\frac{1}{\mu_m}R_o C_1(\mu_m R_o)\right)}{\left(\frac{3}{4}H\right)\left(\frac{1}{2}R_o^2 C_1^2(\mu_m R_o) - R_i^2 C_0^2(\mu_m R_i)\right)} \tag{19}$$

for $n > 1$:

$$A_{mn} = \frac{\left(\frac{1}{\gamma_n^2}(\cos(\gamma_n H) - 1) + \frac{2bH\cos(\gamma_n H)}{\gamma_n^2}\right)\left(\frac{1}{\mu_m}R_o C_1(\eta_m R_o)\right)}{\left(\frac{H}{2}\right)\left(\frac{1}{2}R_o^2 C_1^2(\eta_m R_o) - R_i^2 C_0^2(\eta_m R_i)\right)} \tag{20}$$

Therefore, the solution is complete with all terms known for Eq. (3), and a theoretical temperature response over time may be obtained for any point in the steel plate given a heat input for the previously stated boundary conditions.

$$\begin{aligned}\Theta(r,z,t) = \sum A_{mn}e^{-\alpha(1+\gamma_n^2)t}C_0(\eta_m r)\cos(\gamma_n z) - \left(\frac{q_1''}{k}\right)z \\ + \left(\frac{q_1'' + q_2''}{2kH}\right)z^2 + \left(\frac{q_1'' + q_2''}{\rho c_p H}\right)t\end{aligned} \tag{21}$$

Note that a similar solution can also be derived for the friction plate with the only differences in material properties, thickness and the heat flux inputs.

Series convergence tests have been performed for typical cases. The series solution, Eq. (21), was checked by changing the series from 25×25 terms to 50×50 terms. It was found that the temperature differences only change for less than 1% in initial transient time up to 10 ms, and decrease to less than 0.1% after 50 ms. Thus, 50×50 terms is considered sufficient for the present study and is used throughout.

2.1. Energy partition

The heat generated at the interface of the steel and friction plates is due to the friction force along the contact region caused by the relative motion between the friction and steel plate. The generated heat may either enter the friction or steel plates. Thus, "partitioning" is defined as the fraction of the energy entering the material of interest. This energy partitioning can be obtained by matching the surface temperature at the interface of two different materials as shown by Yuen [18]. For simplicity, a stationary transient one-dimensional semi-infinite solid assumption is made to approximate the temperature distribution in both the steel and friction plates. The general solution of a constant heat flux input at the surface is as follows (Incropera and DeWitt [19]):

$$\Theta(z,t) - \Theta_o = \frac{2q''\sqrt{\frac{\alpha t}{\pi}}}{k}\exp\left(\frac{-z^2}{4\alpha t}\right) - \frac{q''z}{k}\operatorname{erfc}\left(\frac{z}{2\sqrt{\alpha t}}\right) \tag{22}$$

When Eq. (22) is applied at the interface (i.e. $z = 0$), the exponential term and error function term drop since z is zero at the surface. By matching the interface temperature at the steel and friction plates, the following equality can be stated:

$$\left(\frac{q''\sqrt{\alpha}}{k}\right)_s = \left(\frac{q''\sqrt{\alpha}}{k}\right)_f \tag{23}$$

Note that the value of the total heat generated at the interface can be determined experimentally. The heat that enters the friction plate and steel plate is as follows:

$$q''_s = fq'', \quad q''_f = (1-f)q'' \tag{24}$$

The heat partition factor S is determined from the material physical properties as follows:

$$f = \frac{1}{S+1} \text{ where } S = \left(\frac{k_f}{k_s}\right)\sqrt{\frac{\alpha_s}{\alpha_f}} \tag{25}$$

Later, it will be shown that most of the heat generated is transferred to the steel plate. With the known energy partitioning, the heat that enters each of the plates can be estimated, thus the temperature distribution in each plate can be calculated using Eq. (21).

3. Numerical analysis

For the given governing equation (Eq. (1)), the dependent variable temperature can also be solved numerically several different ways. A fully implicit method is used in the present study. An expression for temperature can be found by discretizing the governing equation:

$$\rho c\frac{\Theta_P^{n+1}-\Theta_P^n}{\Delta t} = k\frac{\Theta_N^{n+1}+\Theta_S^{n+1}-2\Theta_P^{n+1}}{\Delta r^2} + k\frac{1}{r_P}\frac{\Theta_N^{n+1}-\Theta_S^{n+1}}{2\Delta r} + k\frac{\Theta_E^{n+1}+\Theta_W^{n+1}-2\Theta_P^{n+1}}{\Delta z^2} \tag{26}$$

In Eq. (26), n represents the previous time and $n+1$ is the current time that is one time step from time n, which can be rearranged in the form:

$$A_N\Theta_N^{n+1} + A_S\Theta_S^{n+1} + A_E\Theta_E^{n+1} + A_W\Theta_W^{n+1} - A_P\Theta_P^{n+1} = -\Theta_P^n \tag{27}$$

where

$$A_N = \frac{\alpha\Delta t}{\Delta r^2} + \frac{1}{r_P}\frac{\alpha\Delta t}{2\Delta r}, \quad A_S = \frac{\alpha\Delta t}{\Delta r^2} - \frac{1}{r_P}\frac{\alpha\Delta t}{2\Delta r},$$

$$A_E = A_W = \frac{\alpha\Delta t}{\Delta z^2}, \quad A_P = \frac{2\alpha\Delta t}{\Delta r^2} + \frac{2\alpha\Delta t}{\Delta z^2} + 1$$

The solution of the finite difference equation (Eq. (26)) is driven by the boundary conditions previously defined (Eq. (2)). For each of the four boundaries considered, a boundary condition of the second type (or Neumann boundary condition) exists in the form of a defined heat flux in the axial direction and zero heat flux in the radial direction. Using a second-order parabolic fit, the general form of the boundary condition for a constant grid reduces to:

$$\left(\frac{\partial\Theta}{\partial n}\right)_n = \frac{-\Theta_{n+2}+4\Theta_{n+1}-3\Theta_n}{2\Delta n} \tag{28}$$

Table 1
Gird convergence test

Grid Size	Time step (s)	Location 1 $z = 0$ mm $r = 88.9$ mm $t = 0.6$ s	Location 2 $z = 1.2$ mm $r = 88.9$ mm $t = 0.6$ s
25 × 25	0.20	14.798 °C	13.805 °C
25 × 25	0.10	14.331 °C	13.405 °C
25 × 25	0.05	14.100 °C	13.209 °C
50 × 50	0.20	14.464 °C	13.492 °C
50 × 50	0.10	14.007 °C	13.101 °C
50 × 50	0.05	13.781 °C	12.909 °C
100 × 100	0.20	14.307 °C	13.345 °C
100 × 100	0.10	13.854 °C	12.957 °C
100 × 100	0.05	13.630 °C	12.767 °C

For an adiabatic case:

$$\Theta_n = \frac{-\Theta_{n+2}+4\Theta_{n+1}}{3} \tag{29}$$

For a given heat flux case:

$$\Theta_n = \frac{-\Theta_{n+2}+4\Theta_{n+1}}{3} + \frac{q_w 2\Delta n}{3k} \tag{30}$$

A line-by-line method is used in this study to compute the matrix generated from Eq. (27). Note that in this case iterations are required to obtain the intermediate $(n+1)^*$ step solution.

3.1. Convergence test

The solution of the finite difference equation, Eq. (26), is obtained iteratively. Differences in point-wise temperatures were used to check the convergence. The error ε between two temperatures at each time step corresponding to consecutive iterations k and $k+1$ are defined as

$$\varepsilon = \frac{|\Theta_{i,j}^{k+1} - \Theta_{i,j}^{k}|}{\Theta_{i,j}^{k+1}} \times 100\% \tag{31}$$

This error must be less than the specified tolerance. In this study the tolerance was set equal to 10^{-5}. To test grid convergence, the time step Δt, the number of nodes in the space coordinate r and z are listed in Table 1. It can be seen from the table that the maximum error was less than 1.2% at location 1 (midpoint of r_i and r_o at surface) and 1.1% at location 2 (midpoint of r_i and r_o and half-thickness), when the mesh size increases from 50 × 50 to 100 × 100 for time step size 0.05 s. Based on the grid convergence test, a time step size of 0.05 s, 50 nodes and 50 nodes in r and z directions is considered sufficient and is used for the calculations presented in this work.

4. Experimental setup

An experiment was carried out using a standard production power-shift transmission consisting of multiple wet-clutch assemblies, one of which being the test subject. The test arrangement included a 746 kW (1000 hp) variable speed DC motor as the prime mover with an external speed

increasing fixed ratio gear box. This gear box output was coupled to the transmission input with a shaft, which included a torque meter. The drive path through the transmission up to the test subject clutch (CLUTCH#5), which includes another engaged clutch (CLUTCH#1) and transfer gear (adjacent to CLUTCH#3). The output from the subject clutch is transferred to the differential gear assembly, which was placed in its lock-up mode to ensure that all torque would be transmitted to the load. The differential output was coupled to the load with a shaft which included a second torque meter. The load consisted of a set of 10 steel plates, each 25.4 mm (1 in.) thick by 762 mm (30 in.) diameter, secured to a shaft.

The steel plates of the test subject clutch were instrumented with thermocouples to measure the temperature changes associated with the engagement process. Detailed dimensions of the steel plates and routing of the thermocouple wires are given in Fig. 4. The thermocouples were installed in the two steel plates noted in Fig. 3. The plates were modified by drilling a 1.56 mm (0.061 in.) radial hole through the steel plate, centered over the 2.64 mm (0.104 in.) thickness, and cross-drilling a hole through the face at half the distance between the inside and outside radii. The cross-drilled hole was then counter-sunk slightly (see Fig. 4) to provide a landing for securing the thermocouple. Also detailed in Fig. 4 is the Type J thermocouple junction welded to the countersunk area, adjacent to the surface. The hole was then filled with a ceramic and the wires were routed down through the clutch hub and shaft, to a slip ring located on the end of the shaft. From the slip ring, the thermocouple wires were connected to a DATAQ DI500 data acquisition card run with a laptop computer containing a 486 processor. Other measurements read in conjunction with the temperatures included the input torque and speed, output torque and speed, and clutch pressure. Both input and output torque measurements were made using strain gauge type torque meters. Each signal was excited and amplified with a separate Daytronic 3200

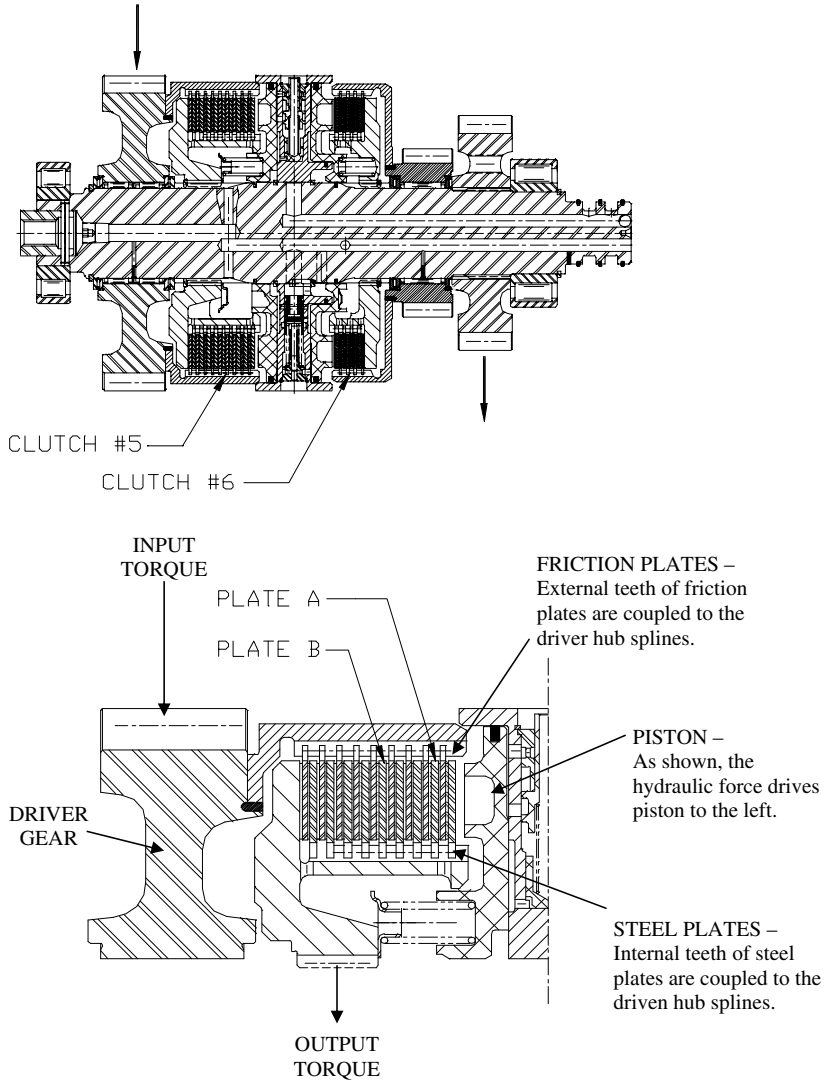

Fig. 3. Test subject clutch and thermocouple plate locations.

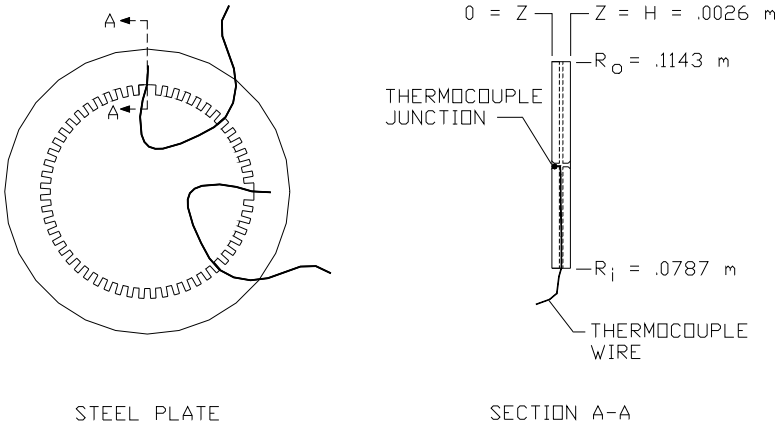

Thermocopule ID	Plate	Position (relative to picture above)
1	A	12:00 position
2	A	3:00 position
3	B	12:00 position
4	B	3:00 position

Fig. 4. Thermocouple locations and plate modifications.

signal conditioner, then fed into the data acquisition card. The input and output speeds were sensed with Hall Effect magnetic pick-ups located above a sprocket on the input shaft and a gear within the transmission on the output side of the subject clutch. Each frequency signal was converted into a voltage with separate Vidar signal conditioners, then fed into the data acquisition card. The clutch actuating pressure was sensed at the oil collector cover of the subject clutch with a stain gauge based pressure transducer. This signal, as with the torque measurements, was excited and amplified with Daytronic 3200 signal conditioners, then fed into the data acquisition card. In summary, a total of nine input signals, or channels, were configured with the data acquisition system. Each channel was configured to record data at a sample rate of 1000 samples per second.

For a typical engagement trial, the motor speed was set constant such that transmission input speed was 1000 rpm while the output inertia load was manually held stationary. With the subject clutch established as the disconnect device, the engagement process began by increasing the oil pressure behind the piston of the subject clutch in a linear ramp profile. The oil pressure was controlled manually with a potentiometer which modulated the current of the solenoid valve for the clutch apply pressure. As the pressure was increased, it reached a point where it combined with the centrifugal pressure effect to overcome the opposing force of the return spring. At this point, with the piston oil pressure approximately 689 kPa (100 psi), the contact between the friction and steel plates was initiated (i.e., beginning of the second stage of engagement). Oil pressure was continually increased in the same linear ramp-like profile until the solenoid valve was fully open. Note that the clutch pressure at which no relative motion between the plates occurred, beginning at the lock-up stage, was approximately 827 kPa (120 psi). Also note that this point of lock-up is unique for this application and would change for a different inertia or different input speed.

5. Results and discussion

The magnitude of the heat generated due to the friction between steel and friction plates can be determined using the data recorded from the experiment trails. Newton's second law of motion governs the torque relationship at the clutch interface. Shigley and Mischke [1] cited the equations of motion for the input and output inertia as Eq. (32), assuming the input and output sides of the clutch have constant inertia values with negligible energy transfer losses.

$$T_{\text{in}} = -I_{\text{in}} \int \frac{\mathrm{d}\omega_{\text{in}}}{\mathrm{d}t}, \quad T_{\text{out}} = I_{\text{out}} \int \frac{\mathrm{d}\omega_{\text{out}}}{\mathrm{d}t} \tag{32}$$

Since the input torque and output torque at the clutch interface must be equal, the general form of the energy equation for heat generation (energy dissipation rate) is as follows:

$$e = \int T \frac{\mathrm{d}\omega}{\mathrm{d}t} \text{ where } \omega = \omega_{\text{in}} - \omega_{\text{out}} \tag{33}$$

The total heat generated (total energy dissipated) for each engagement was formulated from Eqs. (32) and (33) by Howrie [20] and expressed in the following equation:

$$E = \frac{1}{2} \frac{I_{\text{in}} I_{\text{out}} (\omega_{\text{in}}^2 - \omega_{\text{out}}^2)}{I_{\text{out}} \left(1 - \frac{T_{\text{in}}}{T_{\text{d}}}\right) + I_{\text{in}} \left(1 - \frac{T_{\text{out}}}{T_{\text{d}}}\right)} \text{ where } T_{\text{d}} = \mu_{\text{d}} N r_{\text{ave}} F \tag{34}$$

It is important to note that the net clutch engagement force must consider the centrifugal pressure effects of the oil during rotation and the opposing spring force.

With the appropriate assumptions, the heat generated at each interface can be found by dividing the total energy calculated from Eq. (34) by the total number of steel and friction plate interfaces. First it is assumed that the hydraulic loading force is equally distributed across the piston. It is further assumed that the centrifugal hydraulic pressure effects and opposing spring force are equally distributed across the piston face. The net piston force is assumed uniformly transferred throughout the clutch at each interface of the wet clutch. Furthermore, spline drag forces and thermoelastic pressure effects, which may cause localized pressure gradients at interfaces, were neglected for this case.

With known heat generation at the interface, the energy partitioning can be calculated using Eq. (25). Note that the energy partitioning (f) only depends on the thermal properties of the steel and friction plate material (see Eqs. (23)–(25)). The thermal properties of the steel plate and friction plate are given in Table 2. It can be seen that the friction plate material has very poor thermal conductivity in comparison to the thermal conductivity of the steel plate. It is expected that most of the heat should enter the steel plates. The energy partitioning value is found to be at a value of 95%, which means essentially all the heat is transferred to the steel plate.

With the known energy partitioning, the heat entering the steel plate is known. Due to symmetry, the heat that enters the steel plate from the top and bottom surfaces can be considered equal. Thus, Eq. (21) can be further simplified to:

$$\Theta(r,z,t) = \sum A_{mn} e^{-\alpha(1+\gamma_n^2)t} C_0(\eta_m r)\cos(\gamma_n z) - \left(\frac{q''}{2k}\right)z + \left(\frac{q''}{kH}\right)z^2 + \left(\frac{2q''}{\rho c_p H}\right)t \quad (35)$$

where q'' is the heat flux that enters the steel plate. Now, the analytical temperatures can be calculated.

The clutch engagement test was repeated maintaining a consistent engagement time and the two result sets is presented here. In each trial, the motor was run at 1000 rpm and the subject clutch was disconnected and the output inertia was not rotating. Over a period of time less then one second, clutch oil pressure was increased gradually in a ramp profile until full applied pressure was reached (1.38 MPa). The engagement data were compiled and the heat flux into the steel plate was calculated using Eq. (34). A detailed review of the data in Figs. 5 and 6 showed that the clutch lock-up occurred at approximately 0.55 s and 0.52 s, respectively. Note that the input inertia and output inertia were 65 and 36 kg m^2, respectively, while the clutch capacity varied from 0 to 7385 Nm with changing oil pressure. The heat generated at each interface is found by dividing the total energy calculated from Eq. (34) by the total number of the steel and friction plate interfaces (i.e., 18 interfaces). The heat transfer rate to the steel plate at each interface is calculated by multiplying the fraction of the heat entering the steel plate from Eq. (25) (i.e., 0.95 in this case). Figs. 5 and 6 demonstrate the time history of the steel plate heat flux. Since the analytical solution

Table 2
Material physical properties

	Thermal conductivity (W/m/K)	Density (kg/m^3)	Specific heat (J/kg/K)	Thermal diffusivity (m^2/s)
Steel plate	50.0	7860	460	1.38×10^{-5}
Friction plate	0.261	1020	1500	1.70×10^{-7}

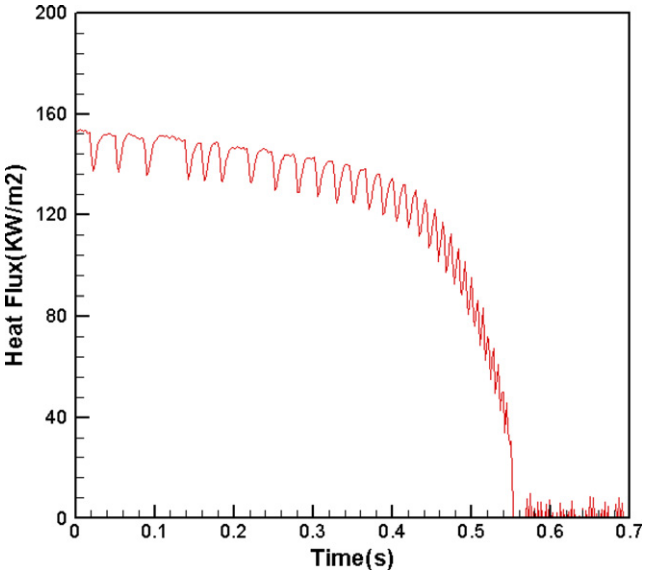

Fig. 5. Time history of steel plate engagement heat flux – Trial 1.

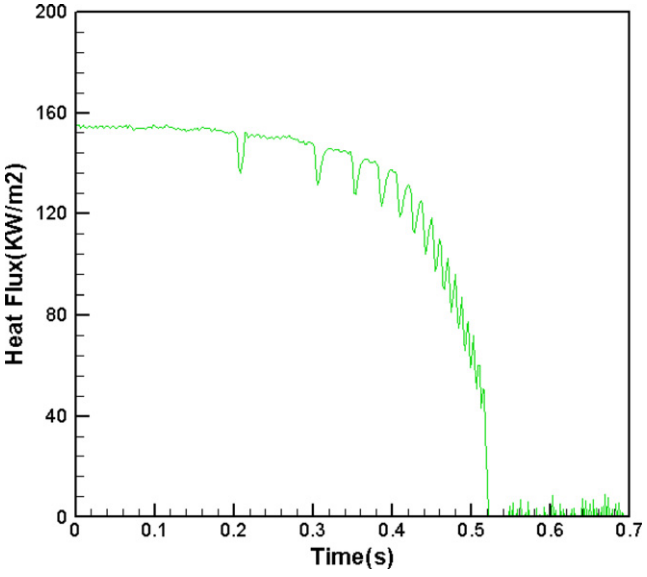

Fig. 6. Time history of steel plate engagement heat flux – Trial 2.

is valid for constant heat flux input, time integration is performed to calculate the averaged heat flux to the steel plate. The averaged heat flux for each trial was found to be 125,950 W/m^2 and 136532 W/m^2. The calculated heat flux was then used in the boundary conditions of the analytical and numerical models previously developed to calculate the temperature rise during one engagement. For the comparison purpose, the surface temperature for the steel plate was calculated at the mean radius. Experimental temperatures T1 and T4 were collected from plate A (see Fig. 3), while temperatures T2 and T3 were collected from plate B. Figs. 7 and 8 shows the comparisons between theoretical analyses and the experimental data. The signal delay in the temperature measured must consider thermocouple junction size, additional slip ring junction and signal conditioning response time. Based on manufacturer specifications of the instrumentation, the delay should be approximately 0.200 s and is factored in Figs. 7 and 8. It can be seen from the figures that the analyses slightly over-predict the steel plate temperature at the mean radius except the temperature near the lock-up time. This may be due to the effect of "boundary lubrication stage" engagement in the early time where there may have some convection effect due to the oil-saturated porous media and the oil passing through the grooves of the friction plate. Also, heat loss from the inside and outside radius surfaces of the steel plate may not be negligible, where an insulated boundary condition was assumed in this study. For measured temperatures, note that there exists a slight temperature rise during the first 0.2 s in Figs. 7 and 8. This is due to the heat generated by the viscous dissipation when two plates squeeze the highly viscous fluid out of the gap between the steel and the friction plates (Jang and Khonsari [11]).

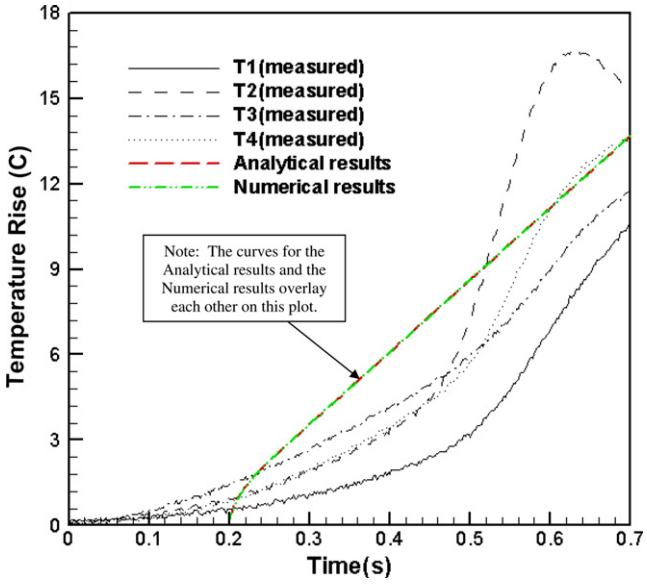

Fig. 7. Temperature measurement considering instrument offset – Trial 1.

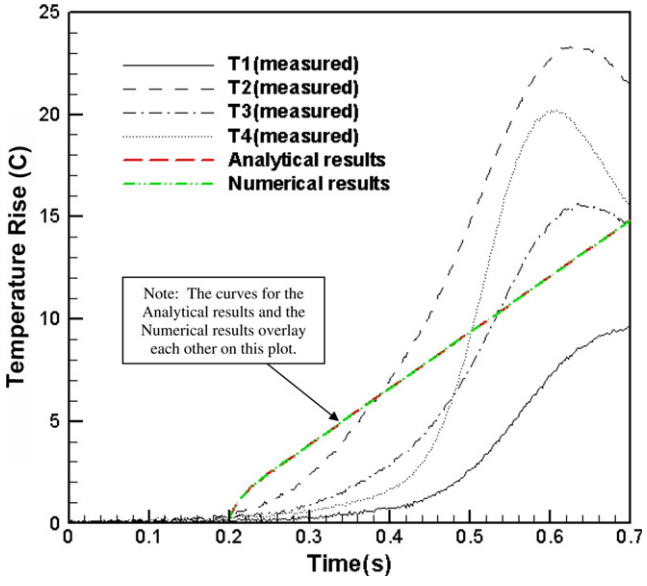

Fig. 8. Temperature measurement considering instrument offset – Trial 2.

Table 3
Comparison of hot spot types

Type	Width (mm)	Temperature (°C)	Duration
Asperity	<1	Up to 1200	<1 ms
Focal	5–20	750–1200	0.5–20 ms
Distortional	20–100	100–700	>10 s
Regional	50–200	10–100	>10 s

Several studies have examined critical temperatures of sliding interfaces leading to thermal failures. Anderson and Knapp [2] took a specific look at hot spotting occurrences in automotive friction systems, including clutches and brakes, due to excessive temperatures caused by the sliding interfaces. They classified four types of hot spotting occurrences as asperity, focal, distortional and regional. These four types are defined by the affected region size and compared in Table 3 (Anderson and Knapp [2]). Based on the data collected in the subject experiment for the engagement duration as shown in Figs. 5–8, the focal type of thermal failure would be of concern. Ramifications of this type could lead to thermal stresses in the steel plate due to the formation of martensite and localized effects on flatness. However, the high temperature ranges noted in Table 3 reflect a case of thermoelastic instability and is beyond the scope of study presented herein.

5.1. Uncertainty analysis

In meeting the objective of this investigation, temperatures of several steel plates were recorded for clutch engagements and compared to analytical and numerical models using a heat flux boundary condition calculated from measured parameters during the same aforementioned clutch engagement. Given that the instrumentation used was properly calibrated to eliminate any fixed or bias error, the validity of the experimental results must consider the random error associated with each measured parame-

Table 4
Wet-clutch uncertainty parameters

Parameter (measured, calculated or referenced)	Uncertainty interval	Confidence limit (%)
Temperature	±1.0 °C	95
Clutch oil pressure	±34.47 kPa	95
Input torque	±15 Nm	95
Output torque	±15 Nm	95
Input speed	±10 rpm	95
Output speed	±10 rpm	95
Input inertia	$\pm 0.65\ kg_m\ m^2$	99
Output inertia	$\pm 0.36\ kg_m\ m^2$	99
Average radius of interface surface	$\pm 2.54 \times 10^{-5}$ m	99
Coefficient of friction	±0.002	95
Friction material thermal conductivity	±0.005 W/m/K	95
Friction material density	$\pm 51\ kg/m^3$	95
Friction material specific heat	±10 J/kg/K	95
Steel plate thermal conductivity	±0.5 W/m/K	95
Steel plate density	$\pm 78\ kg/m^3$	95
Steel plate specific heat	±10 J/kg/K	95

ter. From the normal distribution of the data (Trial 1 was used for this study), an interval where the data will fall can be defined. The likelihood or odds of a measurement falling within the defined interval of the normal distribution must also be made. These two values, defined as the uncertainty interval and confidence limit, are given in Table 4 for each parameter.

The parameters are described as measured, calculated or referenced. This classification is made to better determine all factors in establishing the uncertainty interval for each parameter. For example, the temperature measurement using the Type J thermocouple included the thermocouple junction size and placement on the steel plate, the thermocouple wire, the slip ring, the signal conditioning module and the data acquisition card (which includes analog-to-digital conversion). Although great care was taken in creating the circuit to produce the electromotive force, the error associated with the module in processing the signal was similar to the error associated with the junction, wires and slip ring.

Other measured parameters included clutch oil pressure, input and output torque and speed. The strain gage based transducer used to measure oil pressure had a high degree of accuracy and was insignificant relative the error introduced by the signal conditioner. The torque meter, also strain gage based, did not offer as high of accuracy and had to be accounted for along with the signal conditioning when determining error. The Hall Effect sensor, like the pressure transducer, was very accurate and insignificant relative to the amplifier.

Input and output inertia values are classified as calculated parameters. The error associated with the component inertia values is quite small after several calculations were done, considering the tolerance of the manufactured parts.

Dynamic coefficient of friction values used for this study were taken from test data previously generated for friction material using the SAE friction material test procedure. A significant number of trials have been done on the combination of friction material and steel plate combination, which have been very repeatable. After reviewing numerous coefficient of friction curves, a conservative estimate of the interval was determined to be ±0.01.

Properties of the friction material were obtained from the supplier, and plots were generated for thermal conductivity and specific heat for varying temperature. Given a temperature range of 23–150 °C, the thermal conductivity changed 2% while the specific heat changed 35%. Density of the friction material is the most significant source of uncertainty, since oil impregnates its pores until it becomes saturated during the engagement process. As with the friction material properties, plots for thermal conductivity, specific heat and density of the steel material were generated from reference material considering the same temperature range of the friction material.

With the interval and confidence limits established, the propagation of uncertainty within the calculations of the dynamic torque clutch capacity, heat energy generated and heat energy partitioning can be determined. Beginning with the dynamic torque clutch capacity, recall Eq. (33) and note the independent variables:

$$T_d = \mu_d N r_{ave} F \quad \text{where } T_d = T_d(\mu_d N r_{ave} F) \tag{36}$$

As described in Fox and McDonald [21], the effect that a measurement of an independent variable (x_i) in Eq. (36) has on T_d may be estimated by analogy to the derivative of a function. Defining a variation of an independent variable as δx_i would cause T_d to vary according to:

$$(\delta T_d)_i = \frac{\partial T_d}{\partial x_i}\delta x_i \tag{37}$$

If Eq. (37) is normalized with respect to T_d and noting that the uncertainty interval for x_i is defined as $\delta x_i/x_i$, the uncertainty of each independent variable of the dynamic torque clutch capacity is:

$$U_{T_d,i} = \frac{(\delta T_d)_i}{T_d} = \frac{1}{T_d}\frac{\partial T_d}{\partial x_i}\frac{\delta x_i}{x_i}, \quad x_i = \frac{x_i}{T_d}\frac{\partial T_d}{\partial x_i}\frac{\delta x_i}{x_i} = \frac{x_i}{T_d}\frac{\partial T_d}{\partial x_i}U_{x_i} \tag{38}$$

The estimate of the uncertainty in dynamic clutch torque capacity due to the combined effects of all the independent variable uncertainty intervals is best represented by summing the square of each uncertainty value and taking the square root of that value.

$$U_{T_d} = \left[(U_{T_d,\mu})^2 + (U_{T_d,r_{ave}})^2 + (U_{T_d,F})^2\right]^{0.5} \tag{39}$$

Note that the uncertainty of the number of plates was excluded since no uncertainty exists for that parameter.

This uncertainty analysis procedure is applied to the heat generated (Eq. (33)) in the same manner.

$$E = \frac{1}{2}\frac{I_{in}I_{out}(\omega_{in}^2 - \omega_{out}^2)}{I_{out}\left(1 - \frac{T_{in}}{T_d}\right) + I_{in}\left(1 - \frac{T_{out}}{T_d}\right)} \tag{40}$$

Table 5
Experimental uncertainty

Dynamic clutch torque uncertainty	Thermal energy uncertainty	Heat partition uncertainty
5.20%	6.74%	3.50%

where

$$E = E(I_{\text{in}}, I_{\text{out}}, \omega_{\text{in}}, \omega_{\text{out}}, T_{\text{in}}, T_{\text{out}}, T_{\text{d}})$$

The uncertainty of the heat generated is summarized by:

$$U_{\text{E}} = \Big[(U_{\text{E},I_{\text{in}}})^2 + (U_{\text{E},I_{\text{out}}})^2 + (U_{\text{E},\omega_{\text{in}}})^2 + (U_{\text{E},\omega_{\text{out}}})^2 + \Big(U_{\text{E},T_{\text{in}}})^2 + (U_{\text{E},T_{\text{out}}})^2 + (U_{\text{E},T_{\text{d}}})^2\Big]^{0.5} \tag{41}$$

Likewise, the uncertainty analysis of the heat partition factor begins with Eq. (24).

$$P = \left(\frac{k_{\text{f}}}{k_{\text{s}}}\right)\sqrt{\frac{\alpha_{\text{s}}}{\alpha_{\text{f}}}} \quad \text{or } P = \frac{\sqrt{k_{\text{f}} c_{p_{\text{f}}} \rho_{\text{f}}}}{\sqrt{k_{\text{s}} c_{p_{\text{s}}} \rho_{\text{s}}}} \tag{42}$$

where

$$P = P(k_{\text{f}}, c_{p_{\text{f}}}, \rho_{\text{f}}, k_{\text{s}}, c_{p_{\text{s}}}, \rho_{\text{s}})$$

The uncertainty of the heat partition factor is summarized by:

$$U_{\text{P}} = [(U_{P,k_{\text{f}}})^2 + (U_{P,c_{p_{\text{f}}}})^2 + (U_{P,\rho_{\text{f}}})^2 + (U_{P,k_x})^2 + (U_{P,c_{p_{\text{s}}}})^2 + (U_{P,\rho_{\text{s}}})^2]^{0.5} \tag{43}$$

With the data collected from the Trial 1, all analysis was done for each data point collected and then averaged from the initial condition to the initial point of lock-up. The results of the uncertainty analysis for Eqs. (39), (41) and (43) are summarized in Table 5.

6. Concluding remarks

A combined theoretical and experimental thermal analysis is conducted on the plates within a wet clutch for one engagement. An analytical model using the separation of variables technique was developed to simulate the temperature rise due to the non-conservative friction and relative motion between the steel plates and friction plates of the clutch. The energy partition for the steel and friction plates is evaluated through temperature matching at the interface. A fully implicit finite difference numerical analysis was developed to calculate the temperature distribution in the friction plate. A wet clutch was then instrumented with thermocouples and installed in a power-shift transmission to measure the temperature rise during engagement. Finally, the temperature rises predicted by the analytical and numerical models are compared to the experimental data with reasonable agreements.

The scope of this paper limited the thermal analytical model of the wet clutch engagement with simplifying assumptions and determined the merit with experimental data. As seen in Figs. 7 and 8, the experimental data tracks the predicted data. Given the experimental results are not captured precisely by the model reflect the non-linear nature of the actual engagement process. The non-linear factors include variations in plate-to-plate engagement timing, asperity contact between plates and non-uniform fluid flow between plates. With these and other factors neglected, the test results trend matched closely to the predicted results.

Acknowledgements

Dr. Tien-Chien Jen and Mr. Daniel Nemecek would like to thank Twin Disc Inc. for their financial supports as well as equipment support for carrying out the experiments. Dr. Tien-Chien Jen would also like to acknowledge partial financial support from NSF GOALI DMII-9908324. Acknowledgement is also made to Mr. Gustavo Gutierrez for the assistance in carrying out some part of the numerical analysis.

References

[1] J.E. Shigley, C.R. Mischke, Mechanical Engineering Design, fifth ed., McGraw-Hill, New York, 1989.
[2] A.E. Anderson, R.A. Knapp, Hot spotting in automotive friction systems, Wear 135 (1990) 319–337.
[3] P. Payvar, Laminar heat transfer in the oil groove of a wet clutch, Int. J. Heat Mass Transfer 34 (7) (1991) 1791–1798.
[4] M.L. Hanviland, J.J. Rogers, E.D. Davison, Steady Temperatures and Friction in Lubricated Clutches, SAE Paper No. 642B, Society of Automotive Engineers, Warrendale, PA, 1963.
[5] M.W. Dundore, R.C. Schnieder, Clutch Energy – A Criteria of Thermal Failure, SAE Paper No. 680582, Society of Automotive Engineers, Warrendale, PA, 1968.
[6] C.W. Schade, Clutch Research – An Analytical and Experimental Investigation of Friction Clutches, ATAC Technical Report No. 11336, Detroit Diesel Allison Division of General Motors, Indianapolis, IN, 1971.
[7] M.G. El-Serbiny, T.P. Newcomb, Numerical Simulation of the Engagement Characteristics of a Wet Clutch, in: Proceedings from Institute of Mechanical Engineers Conference, C63/77, London, 1977, p. 85.
[8] P. Zagrodzki, Numerical analysis of temperature fields and thermal stresses in the friction discs of a multidisc wet clutch, Wear 101 (1985) 255.
[9] P. Zagrodzki, Analysis of thermomechanical phenomena in multidisc clutches and brakes, Wear 140 (1990) 291.
[10] S. Natsumeda, T. Miyoshi, Numerical simulation of engagement of paper based wet clutch facing, ASME J. Tribol. 116 (1994) 232.
[11] J.Y. Jang, M.M. Khonsari, Thermal characteristics of a wet clutch, ASME J. Tribol. 121 (1999) 610.
[12] Y. Yang, R.C. Lam, Y.F. Chen, H. Yabe, Modeling of Heat Transfer and Fluid Hydrodynamics for a Multidisc Wet Clutch, SAE Paper No. 950898, Society of Automotive Engineers, Warrendale, PA, 1995.
[13] P.W. Johnson, Computer modeling of the heat transfer in a powershift transmission clutch under slippage, Master of Science Thesis, Mechanical Engineering, Kansas State University, 1987.
[14] D.A. Pacey, Modeling heat transfer in a wet clutch, Ph.D. Dissertation, Engineering, Kansas State University, 1989.
[15] R.A. Tatara, Parviz Payvar, Multiple engagement wet clutch heat transfer model, Numer. Heat Transfer, Part A 42 (2002) 215–231.

[16] Parviz Payvar, P. Majumdar, Developing flow and heat transfer in a rectangular duct with a moving wall, Numer. Heat Transfer, Part A 26 (1994) 17–30.
[17] Yong G. Lai, Simulation of heat-transfer characteristics of wet clutch engagement processes, Numer. Heat Transfer, Part A 33 (1998) 583–597.
[18] W.Y.D. Yuen, Heat conduction in sliding solids, Int. J. Heat Mass Transfer 31 (3) (1988) 637.
[19] F.P. Incropera, D.P. DeWitt, Fundamentals of Heat and Mass Transfer, fourth ed., John Wiley & Sons, New York, 1996.
[20] W.C. Howrie, A Thermal analysis of a wet disk clutch subjected to continuous multiple engagements, Masters Thesis, Rensselaer Polytechnic Institute, Troy, New York, 1987.
[21] R.W. Fox, A.T. McDonald, Introduction to Fluid Mechanics, third ed., John Wiley & Sons, New York, 1985.